Full-Dynamics-Based Bilateral Teleoperation of Hydraulic Robotic Manipulators

Santeri Lampinen, Janne Koivumäki and Jouni Mattila

Abstract— Teleoperated robotic manipulators can augment human capabilities to remotely operate environments which are hard to reach or too dangerous for humans. Furthermore, in teleoperated tasks where heavy objects are manipulated or great forces are needed, a hydraulic slave manipulator may be the only suitable option. Motivated by the recent advances in nonlinear model-based (NMB) control of hydraulic robotic manipulators, *this study proposes* a full-dynamics-based bilateral force-reflected teleoperation, which is designed between a multiple degrees-of-freedom (*n*-DOF) electrical master manipulator and an *n*-DOF hydraulic slave manipulator. Based on the authors' knowledge, this is the first time that such a system is designed for the teleoperation of hydraulic manipulators. The individual controllers for the master and slave manipulators are designed based on the virtual decomposition control (VDC) approach. Furthermore, a communication channel is designed to couple the two manipulators. Very importantly, this allows arbitrary motion and force scaling between the master and slave manipulators. The performance of the proposed method is demonstrated with a full-scale two-DOF hydraulic slave manipulator.

I. INTRODUCTION

Teleoperated robotic systems can augment human capabilities to remotely operate in harsh and hazardous environments where humans cannot (easily) enter. Examples of operations in such environments are, e.g., subsea infrastructure installation and dismantling, operations in nuclear disaster sites and nuclear reactor maintenance and decommissioning. Furthermore, teleoperated operations can be very favourable in traditionally risk-intensive and dangerous industries, such as the construction industry which faces more than 50,000 fatal accidents per year [1]. In all of these cases, it is common that heavy objects are manipulated, and/or a great amount of force is needed to perform a task. Consequently, when significant forces are needed to perform the task, hydraulic actuators are an obvious choice for the teleoperated slave manipulator due to their great power-to-weight ratio. Furthermore, these actuators can benefit robotic systems due to their simplicity, robustness and low cost.

A control design for hydraulic robotic manipulators is a challenging task due to their highly nonlinear dynamic behaviour which can be described by coupled third-order differential equations. As reviewed in [2], stability-guaranteed nonlinear model-based (NMB) control methods can provide the most advanced control performance for multiple degrees-of-freedom (*n*-DOF) hydraulic robotic manipulators. This

is because the methods can provide theoretically sound tools to rigorously address the nonlinear dynamics of hydraulic manipulators.[1] This is the most important property in environmental interaction tasks (contact tasks), as one of the most significant reasons for instability in environmental interaction is that the manipulator's nonlinear dynamics are not considered rigorously [4], [5]. Furthermore, stability is the primary requirement for all control systems, and an unstable system is typically useless and potentially dangerous [6], [7]. However, designing a stable NMB controller for *n*-DOF hydraulic manipulators has been challenging [2]. Only very recently in [8] and [9] (by Koivumäki and Mattila) were *stability-guaranteed NMB control* designs provided for *n*-DOF hydraulic manipulators performing contact tasks. It is obvious that designing a stability-guaranteed NMB controller for a teleoperation system with a heavy-duty hydraulic slave manipulator is an even more multifaceted control design task. This is because 1) the dynamics connection between a heavy-duty hydraulic slave manipulator and a small-scale electrical master manipulator must be addressed, and 2) due to the significant difference in sizes between the slave and master manipulators, motion and force scaling are needed between the manipulators.

Study of haptic teleoperation commenced in the mid-1940s [10] from the need to manipulate objects in harsh and dangerous environments (e.g., the nuclear industry). A teleoperation is a well-established paradigm with electrical systems and has led to a vast and ever-growing number of applications [10], [11]. However, a very limited amount of research is available on teleoperation with hydraulic manipulators; see [12]–[15]. All of the present studies on teleoperation of hydraulic manipulators in [12]–[15] rely on linearised systems models, transfer functions and linear control theory to design teleoperation systems. Evidently, with highly-nonlinear hydraulic systems, this may raise a question about the control system performance in the entire nonlinear operational range; linear control methods can provide tolerable control performance within only a narrow range (at small signal magnitudes) in the nonlinear operational space and become unstable at a larger range [3]. Furthermore, as demonstrated in [8], [9], [16]–[18], significant control performance improvements has been reported for hydraulic

S. Lampinen, J. Koivumäki and J. Mattila are with Tampere University of Technology, Finland. `name.surname@tut.fi`

[1] In NMB control methods, the main idea is to design a specific feedforward term (from the system inverse dynamics) to proactively generate the required actuator forces from the required motion dynamics, such that the *feedforward term* is designed to take care of the major control actions, whereas the system *feedback terms* are used only to overcome uncertainties, to maintain stability, and to address transition issues [3].

systems by full-dynamics-based control designs.

This study provides the preliminary results for the *full-dynamics-based teleoperation* with *n*-DOF hydraulic manipulators. Based on the authors' best knowledge, this is the first time a full-dynamics-based teleoperation with a hydraulic manipulator is proposed *without any linearisation or order reduction*. The proposed method is built on our previously designed state-of-the-art controllers for *n*-DOF hydraulic manipulators (see [8], [9]). The underlying control design for the entire system (the master and slave manipulators) is based on the unique *virtual decomposition control* (VDC) approach, in which the control problem of a complex robotic system can be converted into control problems of dynamically easier-to-handle *modular subsystems* without imposing additional approximations. Also, an *adaptive control* can be employed in the control design, and the stability of the entire system can be addressed at the subsystem level. Furthermore, the proposed method largely follows the *force-reflected bilateral teleoperation method* presented in [19] where the teleoperation system is designed between two identical electrically-operated manipulators. Very importantly, the method in [19] *allows arbitrary motion and force scaling between the manipulators*. As discussed in [11], the dynamics of the human operator and the teleoperation system are tightly coupled; i.e., the stability of the overall system is affected by the human operator dynamics. Thus, the operator dynamics is considered in the control design. The advancement of the proposed method is verified with a full-scale two-DOF hydraulic slave manipulator (a payload of 475 kg at the tip) driven in contact with a flexible environment.

The paper is organised as follows. First, Section II introduces the reader to the necessary mathematical preliminaries. Section III discusses the concept of VDC. Section IV discusses control of master and slave manipulators, and introduces the reader to the proposed teleoperation scheme. Section V demonstrates the control performance of the system with a full-scale hydraulic manipulator. Section VI concludes the paper and discusses future research.

II. MATHEMATICAL PRELIMINARIES

Let an orthogonal coordinate system (called a frame for simplicity) $\{\mathbf{A}\}$ be attached to a rigid body. Furthermore, let the liner/angular velocity vector of that frame be ${}^{\mathbf{A}}V = \begin{bmatrix} {}^{\mathbf{A}}\mathbf{v} & {}^{\mathbf{A}}\omega \end{bmatrix}^T$, where ${}^{\mathbf{A}}\mathbf{v} \in \mathbb{R}^3$ and ${}^{\mathbf{A}}\omega \in \mathbb{R}^3$ denote the linear and angular velocities of frame $\{\mathbf{A}\}$, respectively. Similarly, let the force/moment vector of frame $\{\mathbf{A}\}$ be ${}^{\mathbf{A}}F = \begin{bmatrix} {}^{\mathbf{A}}\mathbf{f} & {}^{\mathbf{A}}\mathbf{m} \end{bmatrix}^T$, where ${}^{\mathbf{A}}\mathbf{f} \in \mathbb{R}^3$ and ${}^{\mathbf{A}}\mathbf{m} \in \mathbb{R}^3$ are the force and moment vectors applied to the origin of frame $\{\mathbf{A}\}$, respectively. This is the common notation used within the VDC approach.

Let frames $\{\mathbf{A}\}$ and $\{\mathbf{B}\}$ be fixed to a common rigid body. Then, the linear/angular velocity and the force/moment vectors can be transformed between frames as

$${}^{\mathbf{B}}V = {}^{\mathbf{A}}\mathbf{U}_{\mathbf{B}}^T \, {}^{\mathbf{A}}V \tag{1}$$

$${}^{\mathbf{A}}F = {}^{\mathbf{A}}\mathbf{U}_{\mathbf{B}} \, {}^{\mathbf{B}}F \tag{2}$$

where ${}^{\mathbf{A}}\mathbf{U}_{\mathbf{B}} \in \mathbb{R}^{6\times6}$ is a force/moment transformation

matrix. Duality between force/moment and linear/angular velocity transformations is implied by Eq. (1) and (2).

Consider frame $\{\mathbf{A}\}$ attached to a rigid freely-moving body. Then, the dynamic forces of that rigid body, expressed in frame $\{\mathbf{A}\}$, can be defined as

$$\mathbf{M_A}\frac{d}{dt}({}^{\mathbf{A}}V) + \mathbf{C_A}({}^{\mathbf{A}}\omega){}^{\mathbf{A}}V + \mathbf{G_A} = {}^{\mathbf{A}}F^* \tag{3}$$

where $\mathbf{M_A} \in \mathbb{R}^{6\times6}$ denotes the mass matrix, $\mathbf{C_A} \in \mathbb{R}^{6\times6}$ the Coriolis and centrifugal terms, and $\mathbf{G_A} \in \mathbb{R}^{\mathbf{6}}$ the gravity vector of the rigid body.

Finally, let ${}^{\mathbf{A}}V_{\mathrm{r}} \in \mathbb{R}^6$ be the required linear/angular velocity vector (a control design vector specified in more detail in Section IV) of ${}^{\mathbf{A}}V \in \mathbb{R}^6$. Then, in view of [3], the linear parameterised (does *not* mean linearisation) expression for the required rigid body dynamics can be written as

$$\mathbf{Y_A}\theta_{\mathbf{A}} \stackrel{def}{=} \mathbf{M_A}\frac{d}{dt}({}^{\mathbf{A}}V_{\mathrm{r}}) + \mathbf{C_A}({}^{\mathbf{A}}\omega){}^{\mathbf{A}}V_{\mathrm{r}} + \mathbf{G_A}. \tag{4}$$

The detailed formulation for $\mathbf{Y_A} \in \mathbb{R}^{6\times13}$ (the regressor matrix) and $\boldsymbol{\theta_A} \in \mathbb{R}^{13}$ (the parameter vector) can be found in [3].

III. VIRTUAL DECOMPOSITION CONTROL

The VDC approach (see [3], [20]) is a unique subsystem-dynamics-based control design method, in which the control of complex robotic systems can be designed locally at the subsystem level *without imposing additional approximations*. VDC takes advantage of a procedure called *virtual decomposition* where the original system is virtually decomposed into modular *subsystems* (objects and open chains), using conceptual *virtual cutting points* (VCPs). VCPs are directed separation interfaces which conceptually cut through a rigid body. At a VCP, two parts resulting from the virtual cut maintain equal positions and orientations. The VCP forms a virtual cutting surface on which six-dimensional force/moment vectors (see Section II) can be exerted from one part to another. [3]

After the virtual decomposition, the decomposed system is represented by a simple oriented graph (SOG). In the SOG, each subsystem represents a *node*, and each VCP represents a *directed edge*, the direction of which defines the force reference direction. *No loop is allowed in an SOG*. The kinematics of the subsystems can be computed by propagating through every subsystem along the direction of the VCP flow in the SOG (from the *source node* towards the *sink node*). Then, using the kinematics, the dynamics of the subsystems can be computed by propagating through every subsystem along the opposite direction of the SOG (from the *sink node* towards the *source node*) using the *Newton–Euler* convention for the dynamics.[2] Finally, the subsystems' control design can be established using the system kinematics and dynamics.

Within VDC, novel concepts of *virtual power flow* (see Definition 2.16 in [3]) and *virtual stability* (see Definition

---

[2]Conventional NMB methods use the *Lagrange dynamics* for the control system design. VDC is the first rigorous control method to take full advantage of *Newton–Euler dynamics*, enabling many significant advantages.

2.17 in [3]) are a vital part of the control design procedure, as they are the actual enablers for the subsystem-dynamics-based control design. *In short*, the virtual power flows can be described as "stability connectors" amongst the subsystems. Individually, the nature of virtual power flows is "stability preventing", in the sense of the Lyapunov functions method. However, when two adjoining subsystems are connected to each other at the location of the VCP, a positive VCP is connected to a negative VCP, and they cancel each other out. Thus, when all subsystems qualify as virtually stable, the stability (and convergence) of the entire system can be proven in view of Theorem 2.1 in [3]. For more details on the virtual stability and its relation to the stability of the entire system, interested readers are referred to [3].

One of the advantages of VDC is that it allows a true modularity in the control systems design. This is realised in the functionality where changing the control (or dynamics) of one subsystem does not affect the control equations of the rest of the system [3]. Furthermore, then the designed control system (composing of subsystems) can be considered a subsystem of a greater system, as long as their connection is properly handled with VPFs.

As a conclusion, the following steps are performed in the implementation of VDC in robotic systems:

Step 1: Virtual decomposition of the original (complex) system to the subsystems, and presenting the dynamic connections amongst the subsystems in SOG.

Step 2: Description of the subsystems' kinematics by propagating recursively from the base towards the tip (along the direction of the VCP flow in the SOG).

Step 3: Based on the kinematics, description of the subsystems' dynamics by propagating recursively from the tip towards the base (along the opposite direction of the VCP flow in the SOG).

Step 4: Based on the kinematics and dynamics, the NMB control is designed for the decomposed subsystems.

Step 5: Ensuring that all subsystems qualify as virtually stable in the sense of Definition 2.17 in [3], which eventually leads to the stability of the entire system.

IV. THE CONTROL DESIGN

In this section, the control design for the master manipulator is designed in Section IV-A. Then, Section IV-B provides the control design for the slave manipulator. Finally, the connection of the two manipulators for the force-reflected bilateral teleoperation is given in Section IV-C

A. The Control Design for the Master Manipulator

1) Modelling the Human Operator: The human operator is modelled with a two-order linear time invariant model. According to [21], [22], the following model is found effective for modelling human arm dynamics:

$$\mathbf{M}_h \ddot{\mathbf{x}}_h + \mathbf{D}_h \dot{\mathbf{x}}_h + \mathbf{K}_h \mathbf{x}_h = \mathbf{f}_m - \mathbf{f}_h^* \qquad (5)$$

where $\mathbf{M}_h$, $\mathbf{D}_h$ and $\mathbf{K}_h$ are symmetric positive-definite matrices defining the inertia, damping and stiffness of the human operator, respectively; $\mathbf{f}_m$ denotes the reaction force/moment
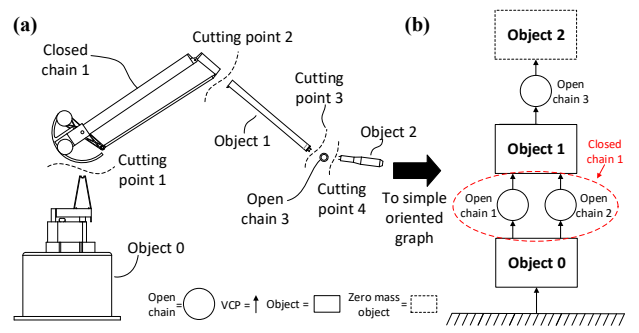

Fig. 1.   a) Virtual decomposition of the master manipulator. b) The SOG of the master manipulator.

vector exerted from the master manipulator towards the operator, $\mathbf{x}_h$ is the position/orientation vector of the human operator's arm and $\dot{\mathbf{x}}_h$ and $\ddot{\mathbf{x}}_h$ are the first and second time-derivatives of the position/orientation vector, respectively. Finally, $\mathbf{f}_h^* \in \mathbb{R}^6$ denotes the exogenous force/moment vector generated by the human operator.

The dynamics of a real human operator are much more complicated and vary amongst different operators, depending on the operators' posture and many other things. The dynamics equation given in (5) is only an approximation of the real dynamics. [3, p.310]

The handle of the master is connected to the rest of the manipulator with a 3-DOF unactuated wrist, notably simplifying modelling of the operator dynamics, because moments do not pass from the operator towards the master manipulator and vice versa. The velocity of the operator's hand and the reaction force from the operator towards the master manipulator are expressed in the handle of the master manipulator as

$$^{\mathbf{S_{tcp}}}F = \mathbf{f}_m \qquad (6)$$

$$^{\mathbf{S_{tcp}}}V = \dot{\mathbf{x}}_h. \qquad (7)$$

2) Virtual Decomposition of the Master Manipulator: The virtual decomposition of the master manipulator is shown in Fig. 1a. The SOG of the system is shown in Fig. 1. The master manipulator comprises one kinematic closed chain and one open chain. Hence, the closed chain is further decomposed into two open chains as shown in Fig. 2. The frame attachment (to describe the system motion and force specifications) to the decomposed system is shown in Fig. 3.

The kinematics and dynamics of the last object are ignored in the scope of this study, and the dynamics of the handle is considered as part of the dynamics of the operator. Forces applied by the operator are considered to be applied directly to the frame $\{S_{\mathbf{tcp}}\}$.

3) Kinematics: The linear/angular velocity vectors of the *fixed and stationary* frames $\{\mathbf{B_{cc}}\}$, $\{\mathbf{B_1}\}$ and $\{\mathbf{B_2}\}$ are known and can be written as

$$^{\mathbf{B_{cc}}}V = {}^{\mathbf{B_1}}V = {}^{\mathbf{B_2}}V = [0\ 0\ 0\ 0\ 0\ 0]^T. \qquad (8)$$

In view of (1) and Fig. 2, the linear/angular velocity vectors of open chain 1 can be computed as

$$^{\mathbf{B_{11}}}V = {}^{\mathbf{B_1}}\mathbf{U}_{\mathbf{B_{11}}}^T\ {}^{\mathbf{B_1}}V + \mathbf{z}_\tau \dot{\theta}_2 \qquad (9)$$
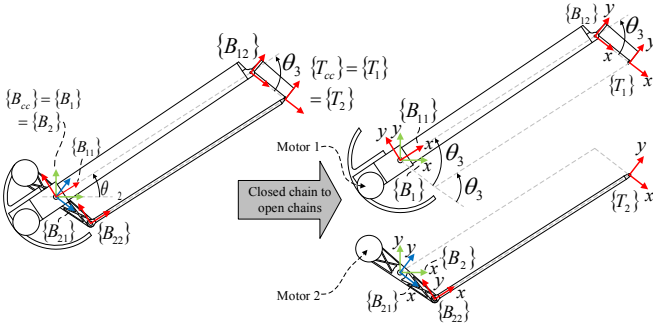
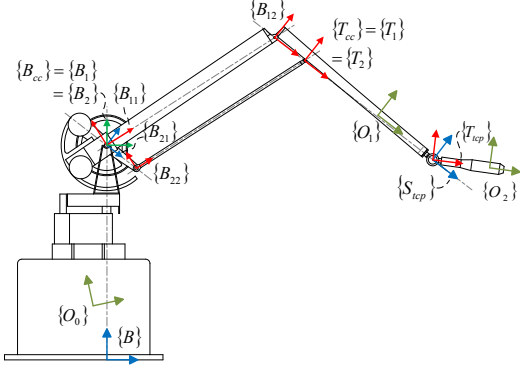Fig. 2.   Decomposition of *closed chain* 1 into two *open chains*.

Fig. 3.   Frame assignment of the master manipulator.

$$\mathbf{^{B_{12}}}V = \mathbf{^{B_{11}}U_{B_{12}}^T}\ \mathbf{^{B_{11}}}V + \mathbf{z}_\tau \dot{\theta}_3 \tag{10}$$

$$\mathbf{^{T_1}}V = \mathbf{^{B_{12}}U_{T_1}^T}\ \mathbf{^{B_{12}}}V \tag{11}$$

where $\mathbf{z}_\tau = [0\ 0\ 0\ 0\ 0\ 1]^T$. Accordingly, the linear/angular velocities of open chain 2 can be computed as

$$\mathbf{^{B_{21}}}V = \mathbf{^{B_2}U_{B_{21}}^T}\ \mathbf{^{B_2}}V + \mathbf{z}_\tau(\dot{\theta}_2 + \dot{\theta}_3) \tag{12}$$

$$\mathbf{^{B_{22}}}V = \mathbf{^{B_{21}}U_{B_{22}}^T}\ \mathbf{^{B_{21}}}V - \mathbf{z}_\tau \dot{\theta}_3 \tag{13}$$

$$\mathbf{^{T_2}}V = \mathbf{^{B_{22}}U_{T_2}^T}\ \mathbf{^{B_{22}}}V + \mathbf{z}_\tau \dot{\theta}_3. \tag{14}$$

Finally, the linear/angular velocity of the frame $\{\mathbf{O_1}\}$ can be computed as

$$\mathbf{^{T_{cc}}}V = \mathbf{^{T_1}}V = \mathbf{^{T_2}}\ V \tag{15}$$

$$\begin{aligned}\mathbf{^{O_1}}V &= \mathbf{^{T_{cc}}U_{O_1}^T}\ \mathbf{^{T_{cc}}}V \\ &= \mathbf{^{S_{tcp}}U_{O_1}^T}\ \mathbf{^{S_{tcp}}}V.\end{aligned} \tag{16}$$

4) Dynamics: The dynamics of *object 1* can be written using (3) with appropriate frame substitutions as

$$\mathbf{M_{O_1}}\frac{d}{dt}(\mathbf{^{O_1}}V) + \mathbf{C_{O_1}}(\mathbf{^{O_1}}\omega)\mathbf{^{O_1}}V + \mathbf{G_{O_1}} = \mathbf{^{O_1}}F^* \tag{17}$$

where $\mathbf{^{O_1}}V \in \mathbb{R}^6$ is obtained from (16). Then, the force resultant equation *object 1* (and the force/moment vector $\mathbf{^{T_{cc}}}F$ at *cutting point 2*) can be written as

$$\mathbf{^{T_{cc}}}F = \mathbf{^{T_{cc}}U_{O_1}}\ \mathbf{^{O_1}}F^* + \mathbf{^{T_{cc}}U_{S_{tcp}}}\ \mathbf{^{S_{tcp}}}F \tag{18}$$

where $\mathbf{^{S_{tcp}}}F$ denotes the external force vector exerted by the human operator towards the handle of the manipulator.

Similar to (17), the rigid body dynamics of the four rigid links in *closed chain 1* can be computed in view of (17) as

$$\mathbf{M_A}\frac{d}{dt}(\mathbf{^A}V) + \mathbf{C_A}(\mathbf{^A}\omega)\mathbf{^A}V + \mathbf{G_A} = \mathbf{^A}F^* \tag{19}$$

by substituting frames $\{\mathbf{B_{11}}\}$, $\{\mathbf{B_{12}}\}$, $\{\mathbf{B_{21}}\}$ and $\{\mathbf{B_{22}}\}$ for

frame $\{\mathbf{A}\}$. Next, the following assumption is made.

Assumption 1. *The frictional torques of each unactuated joints in the master manipulator are considered zero.*

In view of Assumption 1, torque constraints in the unactuated joints can be written as

$$\mathbf{z}_\tau^T\mathbf{^{B_{12}}}F = 0 \tag{20}$$

$$\mathbf{z}_\tau^T\mathbf{^{B_{22}}}F = 0 \tag{21}$$

$$\mathbf{z}_\tau^T\mathbf{^{T_2}}F = 0. \tag{22}$$

The force/moment vector at *cutting point 2* can be divided amongst *open chain 1* and *open chain 2* as

$$\mathbf{^{T_{cc}}}F = \mathbf{^{T_1}}F + \mathbf{^{T_2}}F \tag{23}$$

Furthermore, the force/moment vectors $\mathbf{^{T_1}}F$ and $\mathbf{^{T_2}}F$ of the two *open chains* are written as

$$\mathbf{^{T_1}}F = \alpha_1 \mathbf{^{T_{cc}}}F + \mathbf{^{T_{cc}}}\eta \tag{24}$$

$$\mathbf{^{T_2}}F = \alpha_2 \mathbf{^{T_{cc}}}F - \mathbf{^{T_{cc}}}\eta \tag{25}$$

where load distribution factors α_1 and α_2 (by geometric conditions), with the property of $\alpha_1 + \alpha_2 = 1$, and an internal force vector $\mathbf{^{T_{cc}}}\eta \in \mathbb{R}^6$ can be solved by following the procedure presented in [23], such that the joint torque constraints (20)–(22) are satisfied.

Then, using (19) with $\{\mathbf{B_{11}}\}$ and $\{\mathbf{B_{12}}\}$, the force/moment vectors in *open chain 1* can be written as

$$\mathbf{^{B_{12}}}F = \mathbf{^{B_{12}}}F^* + \mathbf{^{B_{12}}U_{T_1}}\ \mathbf{^{T_1}}F \tag{26}$$

$$\mathbf{^{B_{11}}}F = \mathbf{^{B_{11}}}F^* + \mathbf{^{B_{11}}U_{B_{12}}}\ \mathbf{^{B_{12}}}F \tag{27}$$

$$\mathbf{^{B_1}}F = \mathbf{^{B_1}U_{B_{11}}}\ \mathbf{^{B_{11}}}F \tag{28}$$

and, similarly, using (19) with $\{\mathbf{B_{21}}\}$ and $\{\mathbf{B_{22}}\}$, the force/moment vectors in *open chain 2* can be computed as

$$\mathbf{^{B_{22}}}F = \mathbf{^{B_{22}}}F^* + \mathbf{^{B_{22}}U_{T_1}}\ \mathbf{^{T_2}}F \tag{29}$$

$$\mathbf{^{B_{21}}}F = \mathbf{^{B_{21}}}F^* + \mathbf{^{B_{21}}U_{B_{22}}}\ \mathbf{^{B_{22}}}F \tag{30}$$

$$\mathbf{^{B_2}}F = \mathbf{^{B_2}U_{B_{21}}}\ \mathbf{^{B_{21}}}F. \tag{31}$$

Finally, motor 1 torque τ_{M1} around frame $\{\mathbf{B_{11}}\}$, affecting *open chain 1*, and motor 2 torque τ_{M2} around frame $\{\mathbf{B_{21}}\}$, affecting *open chain 2*, can be written as

$$\tau_{M1} = \mathbf{z}_\tau^T\ \mathbf{^{B_{11}}}F \tag{32}$$

$$\tau_{M2} = \mathbf{z}_\tau^T\ \mathbf{^{B_{21}}}F. \tag{33}$$

5) Control Equations: For the required linear/angular velocity vectors of the manipulator, the required joint velocities must be defined. They can be derived from the required velocity of the master manipulator tip as

$$[\dot{\theta}_{2r}\ \dot{\theta}_{3r}]^T = \mathbf{J}^{-1}\mathbf{v}_{mr} \tag{34}$$

where $\mathbf{v}_{mr}$ is the required velocity of the master manipulator tip, expressed in frame $\{\mathbf{B}\}$, and $\mathbf{J}$ is the Jacobian matrix. *The control design variable $\mathbf{v}_{mr}$ is specified in more detail in (62) in Section IV-C.*

The required velocity of the fixed frame $\{\mathbf{B_1}\}$ can be written as

$$\mathbf{^{B_{cc}}}V_r = \mathbf{^{B_1}}V_r = \mathbf{^{B_2}}V_r = [0\ 0\ 0\ 0\ 0\ 0]^T. \tag{35}$$

The required linear/angular velocity vectors in *open chain 1*

can be written as

$$^{\mathbf{B_{11}}}V_r = {}^{\mathbf{B_1}}\mathbf{U}_{\mathbf{B_{11}}}^T \, {}^{\mathbf{B_1}}V_r + \mathbf{z}_\tau \dot{\theta}_{2r} \tag{36}$$

$$^{\mathbf{B_{12}}}V_r = {}^{\mathbf{B_{11}}}\mathbf{U}_{\mathbf{B_{12}}}^T \, {}^{\mathbf{B_{11}}}V_r + \mathbf{z}_\tau \dot{\theta}_{3r} \tag{37}$$

$$^{\mathbf{T_1}}V_r = {}^{\mathbf{B_{12}}}\mathbf{U}_{\mathbf{T_1}}^T \, {}^{\mathbf{B_{12}}}V_r. \tag{38}$$

Similarly, the required linear/angular velocities in *open chain 2* can be written as

$$^{\mathbf{B_{21}}}V_r = {}^{\mathbf{B_2}}\mathbf{U}_{\mathbf{B_{21}}}^T \, {}^{\mathbf{B_2}}V_r + \mathbf{z}_\tau (\dot{\theta}_{2r} + \dot{\theta}_{3r}) \tag{39}$$

$$^{\mathbf{B_{22}}}V_r = {}^{\mathbf{B_{21}}}\mathbf{U}_{\mathbf{B_{22}}}^T \, {}^{\mathbf{B_{21}}}V_r - \mathbf{z}_\tau \dot{\theta}_{3r} \tag{40}$$

$$^{\mathbf{T_2}}V_r = {}^{\mathbf{B_{22}}}\mathbf{U}_{\mathbf{T_2}}^T \, {}^{\mathbf{B_{22}}}V_r + \mathbf{z}_\tau \dot{\theta}_{3r}. \tag{41}$$

Finally, the required linear/angular velocity at the frames $\{\mathbf{O_1}\}$ and $\{\mathbf{B_{tcp}}\}$ can be written as

$$^{\mathbf{T_{cc}}}V_r = {}^{\mathbf{T_1}}V_r = {}^{\mathbf{T_2}}V_r \tag{42}$$

$$^{\mathbf{O_1}}V_r = {}^{\mathbf{T_{cc}}}\mathbf{U}_{\mathbf{O_1}}^T \, {}^{\mathbf{T_{cc}}}V_r$$
$$= {}^{\mathbf{S_{tcp}}}\mathbf{U}_{\mathbf{O_1}}^T \, {}^{\mathbf{S_{tcp}}}V_r. \tag{43}$$

After defining the required linear/angular velocity vectors in (35)–(43), the required control laws for the system dynamics should be defined. The required contact force towards the operator is defined in [19] as

$$f_{mr} = \mathbf{M}_h \dot{\mathbf{v}}_{mr} + \mathbf{D}_h \dot{\mathbf{x}}_h + \mathbf{K}_h \mathbf{x}_h + \alpha_h \mathrm{sgn}\left(\mathbf{v}_{mr} - \mathbf{v}_m\right). \tag{44}$$

The last term on the right hand side of (44) is a velocity feedback term intended to compensate uncertain exogenous operator force. However, the switching nature of the feedback term may cause instability [24].

Instead of using the switching term to ensure stability, the exogenous force of the operator is estimated with a fast parameter adaptation function as suggested in [25]. Thus, the required reaction force of the handle is written as

$$^{\mathbf{S_{tcp}}}F_r = \mathbf{M}_h \dot{\mathbf{v}}_{mr} + \mathbf{D}_h \dot{\mathbf{x}}_h + \mathbf{K}_h \mathbf{x}_h + \hat{\mathbf{f}}_h^* \tag{45}$$

where $\hat{\mathbf{f}}_h^*$ denotes the estimate of the exogenous force exerted by the operator towards the handle of the master manipulator.

The required net force/moment vectors for each rigid link and object can be designed using the specified required linear/angular velocity vectors in (35)–(43). The required net force/moment vector comprises the model-based feedforward term, that compensates the dynamic forces, and velocity feedback term between the measured velocity and the required velocity. The required net force/moment vectors for the master manipulator can be written as

$$^{\mathbf{A}}F_r^* = \mathbf{Y}_{\mathbf{A}}\theta_{\mathbf{A}} + \mathbf{K}_{\mathbf{A}}\left(^{\mathbf{A}}V_r - {}^{\mathbf{A}}V\right) \tag{46}$$

by substituting frames $\{\mathbf{O_1}\}$, $\{\mathbf{B_{11}}\}$, $\{\mathbf{B_{12}}\}$, $\{\mathbf{B_{21}}\}$ and $\{\mathbf{B_{22}}\}$ for frame $\{\mathbf{A}\}$. Furthermore, in (46), the first term on the right hand side is the model-based feedforward term defined in (4), and the second term is the velocity feedback term, where $\mathbf{K}_{\mathbf{A}}$ is a diagonal positive definite gain matrix.

Consider that all of the system-required net force/moment vectors are known by (46). Next, the required force/moment vectors (force resultants) at the system frames can be computed by propagating to the opposite direction of the SOG, beginning from object 1. In view of (18), the required force resultant equation of *object 1* can be written as

$$^{\mathbf{T_{cc}}}F_r = {}^{\mathbf{T_{cc}}}\mathbf{U}_{\mathbf{O_1}} \, {}^{\mathbf{O_1}}F_r^* + {}^{\mathbf{T_{cc}}}\mathbf{U}_{\mathbf{S_{tcp}}} \, {}^{\mathbf{S_{tcp}}}F_r \tag{47}$$

and in view of (23), the required force/moment vector at VCP 2 can be written as

$$^{\mathbf{T_{cc}}}F_r = {}^{\mathbf{T_1}}F_r + {}^{\mathbf{T_2}}F_r. \tag{48}$$

The required counterparts of the joint constraints, under Assumption 1, can be written as

$$\mathbf{z}_\tau^{T\mathbf{B_{12}}} F_r = 0 \tag{49}$$

$$\mathbf{z}_\tau^{T\mathbf{B_{22}}} F_r = 0 \tag{50}$$

$$\mathbf{z}_\tau^{T\mathbf{T_2}} F_r = 0. \tag{51}$$

In view of (24)–(31), the required force/moment vectors in *open chain* 1 and 2 can be written as

$$^{\mathbf{T_1}}F_r = \alpha_1 {}^{\mathbf{T_{cc}}}F_r + {}^{\mathbf{T_{cc}}}\eta_r \tag{52}$$

$$^{\mathbf{B_{12}}}F_r = {}^{\mathbf{B_{12}}}F_r^* + {}^{\mathbf{B_{12}}}\mathbf{U}_{\mathbf{T_1}} \, {}^{\mathbf{T_1}}F_r \tag{53}$$

$$^{\mathbf{B_{11}}}F_r = {}^{\mathbf{B_{11}}}F_r^* + {}^{\mathbf{B_{11}}}\mathbf{U}_{\mathbf{B_{12}}} \, {}^{\mathbf{B_{12}}}F_r \tag{54}$$

$$^{\mathbf{T_2}}F_r = \alpha_2 {}^{\mathbf{T_{cc}}}F_r - {}^{\mathbf{T_{cc}}}\eta_r \tag{55}$$

$$^{\mathbf{B_{22}}}F_r = {}^{\mathbf{B_{22}}}F_r^* + {}^{\mathbf{B_{22}}}\mathbf{U}_{\mathbf{T_2}} \, {}^{\mathbf{T_2}}F_r \tag{56}$$

$$^{\mathbf{B_{21}}}F_r = {}^{\mathbf{B_{21}}}F_r^* + {}^{\mathbf{B_{21}}}\mathbf{U}_{\mathbf{B_{22}}} \, {}^{\mathbf{B_{22}}}F_r. \tag{57}$$

In (52) and (55), α_1, α_2 and $^{\mathbf{T_{cc}}}\eta_r$ can be obtained by following the procedure presented in [23].

Finally, the required actuating forces of the manipulator can be written as

$$\tau_{M1} = \mathbf{z}_\tau^T \, {}^{\mathbf{B_{11}}}F_r \tag{58}$$

$$\tau_{M2} = \mathbf{z}_\tau^T \, {}^{\mathbf{B_{21}}}F_r. \tag{59}$$

6) Exogenous Force Estimation: Direct dynamics-based force estimation is used to estimate the exogenous forces at the handle of the master manipulator. This method requires well known dynamics of the manipulator, as well as the joint velocities and accelerations. Within this work, they are acquired by differentiating from the joint angles. For higher accuracy and less noise, an acceleration sensor could be used to measure joint accelerations directly.

Extraction of the torques related to the external forces applied by the operator is done by comparing the applied motor torques to the dynamics of the robot as

$$\tau_{ext} = \mathbf{M}\frac{d}{dt}(V) + \mathbf{C}(\omega)V + \mathbf{G} - \tau_m \tag{60}$$

where τ_{ext} is the torques related to the external force, τ_m is the applied torques and $\mathbf{M}\frac{d}{dt}(V) + \mathbf{C}(\omega)V + \mathbf{G}$ is the dynamics of the robot as shown in the previous subsection. The estimate of the reaction force at the handle of the master manipulator is used later in the teleoperation scheme.

B. Control of the Slave Manipulator

Control of the slave manipulator is done in a similar manner as that of the master manipulator with the exception of the control of hydraulic actuators. Fig. 4 (a) shows the structure of the hydraulic slave manipulator, (b) the virtual decomposition of the system and (c) the simple oriented graph. The control design for the part inside the dashed line in Fig. 4 (c) can be found in [8]. The full-model-based control for object 2 is designed using the rigid body dynamics (similarly as described for object 1 in Section IV-A.5), and using *the required Cartesian space control input*
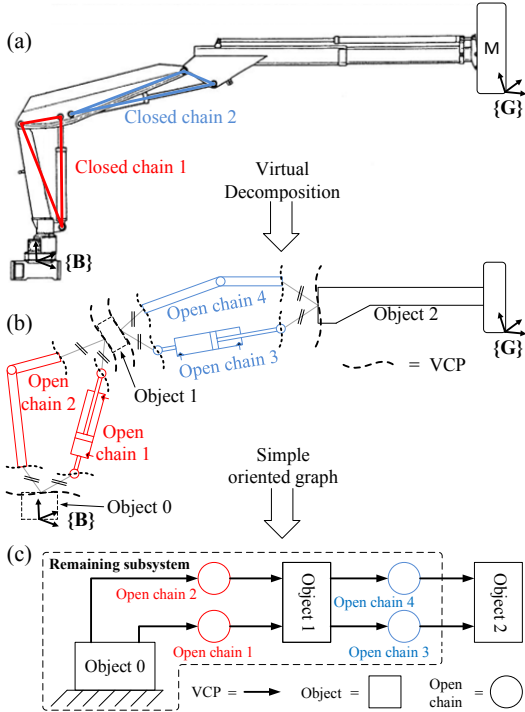
Fig. 4. a) The hydraulic slave manipulator. b) Virtual decomposition of the slave. c) The SOG of the slave.

Fig. 5. Experimental implementation.

(61) *addressed later in Section IV-C.*

As is well known, contact control requires force feedback (i.e., the contact force measurement). However, the use of a conventional six-DOF force/moment sensor at the manipulator tip is not practical as hydraulic manipulators can generate a great amount of force and conventional sensors (built using either strain-gauge technology or optics) are sensitive to shocks and overloading. To prevent the use of these fragile sensors, a method for estimating the contact forces from the chamber pressures of the system actuators was developed in [8]. *This method is also used in the present study.* Discussion of the inherent inaccuracies of the force estimation method can be found in [8], [9].

C. Teleoperation

As shown in the previous sections, individual motion/force controllers have been designed for both master and slave manipulator. *The teleoperation system can be completed by designing the communication channel between master and slave manipulators* [19]. This is done with specific designs for $\mathbf{v}_{mr} \in \mathbb{R}^6$ and $\mathbf{v}_{sr} \in \mathbb{R}^6$. This approach to teleoperation is similar to four-channel architecture in [26], but instead of single inverse dynamics control, both plants are controlled separately, subject to independent motion/force control.

In line with [19], $\mathbf{v}_{sr}$ and $\mathbf{v}_{mr}$ are written as

$$\mathbf{v}_{sr} = \kappa_p \tilde{\mathbf{v}}_m + \Lambda\big(\kappa_p \tilde{\mathbf{p}}_m - \mathbf{p}_s\big) - \mathbf{A}\big(\tilde{\mathbf{f}}_s + \kappa_f \tilde{\mathbf{f}}_m\big) \quad (61)$$

$$\mathbf{v}_{mr} = \kappa_p^{-1} \tilde{\mathbf{v}}_s + \Lambda\big(\kappa_p^{-1} \tilde{\mathbf{p}}_s - \mathbf{p}_m\big) - \mathbf{A}\kappa_p^{-1}\big(\tilde{\mathbf{f}}_s + \kappa_f \tilde{\mathbf{f}}_m\big) \, (62)$$

where κ_f and κ_p are position and force scaling factors *for arbitrary motion/force scaling between the manipulators;* $\Lambda \in \mathbb{R}^{6 \times 6}$ and $\mathbf{A} \in \mathbb{R}^{6 \times 6}$ are diagonal positive-definite matrices; $\mathbf{p}_m \in \mathbb{R}^6$ and $\mathbf{p}_s \in \mathbb{R}^6$ denote the position/orientation
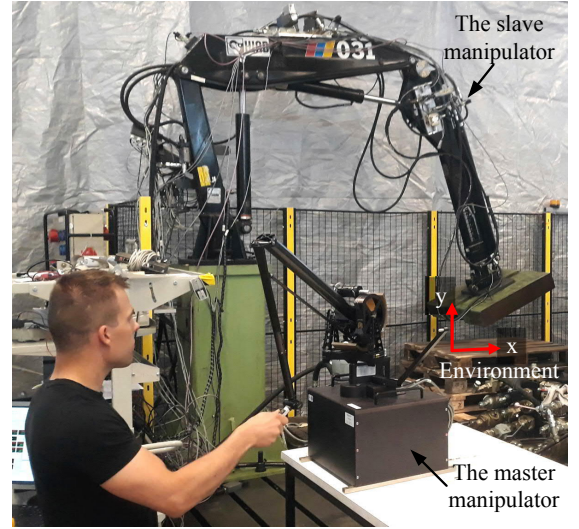
of the master and slave manipulator, respectively, subject to $\dot{\mathbf{p}}_m = \mathbf{v}_m$ and $\dot{\mathbf{p}}_s = \mathbf{v}_s$; and filtered vectors $\tilde{\mathbf{v}}_m$, $\tilde{\mathbf{v}}_s$, $\tilde{\mathbf{p}}_m$, $\tilde{\mathbf{p}}_s$, $\tilde{\mathbf{f}}_m$ and $\tilde{\mathbf{f}}_s$ can obtained with first order filter as

$$\dot{\tilde{\mathbf{z}}} + \mathbf{C}\tilde{\mathbf{z}} = \mathbf{C}\mathbf{z}, \quad \forall \mathbf{z} \in \{\mathbf{v}_m, \mathbf{v}_s, \mathbf{p}_m, \mathbf{p}_s, \mathbf{f}_m, \mathbf{f}_s\} \quad (63)$$

where $\mathbf{C} \in \mathbb{R}^{6 \times 6}$ is a diagonal positive definite matrix.

The use of filtered variables in the two design vectors, (61) and (62), makes the required accelerations $\dot{\mathbf{v}}_{sr}$ and $\dot{\mathbf{v}}_{mr}$, functions of $\mathbf{v}_m$, $\mathbf{v}_s$, $\mathbf{f}_m$ and $\mathbf{f}_s$. This indicates that no acceleration measurement is required from this aspect. However, the use of external force estimators on both plants makes acceleration measurement required, to have valid estimates of the dynamical forces.

Stability of the teleoperation system with the above defined design vectors is shown in [19]. It is shown that the velocities of the manipulators remain bounded for bounded exogenous forces in free space, in contact with flexible/rigid environment, and in contact with rigid and flexible environment at the same time. This is uncommon approach within teleoperation systems, where passivity of the overall system is traditionally used.

The realized teleoperation system is not perfectly transparent in the sense of ideal kinesthetic coupling [27], but acts as a virtual tool by which the operator can interact with the environment. Apparent mass and damping of the virtual tool are solely dependent of control and scaling parameters. The mass and damping of the virtual tool are set to as low as possible to achieve better perceived transparency of the system. However, the mass and damping of the virtual tool cannot be lowered limitless, but a trade-off between stability and transparency has to be made. Very importantly, the asymptotic motion tracking between the master and slave manipulators can be guaranteed in both free-space and constrained motions by following the control design principles in [3], [19].

V. THE EXPERIMENTS

This section presents the experimental test setup (in Section V-A) and provides the experimental results with the proposed teleoperation system (in Section V-B).

A. Experimental Setup

Fig. 5 shows the experimental setup. The experimental implementation comprises four main components, visualised in Fig. 6, which are the master manipulator, the host computer for the master manipulator, the main control computer and the slave manipulator. The Phantom Premium 6DOF/3.0L haptic manipulator is used as the master manipulator, whilst the HIAB-031 hydraulic manipulator is used as a slave manipulator. The controllers of the master and slave manipulators are discussed in Section III. The two-DOF hydraulic manipulator (in Fig. 5) has a maximum reach of approximately 3.2 m, and a payload of 475 kg is attached to its tip. The workspace of the slave can be found in [17] (note that in the present study the telescopic boom was disabled). For the real-time control system, the following components were used: a DS1005 processor board, DS3001 incremental encoder board, DS2103 DAC board, DS2003 ADC board, and DS4504 100 Mb/s ethernet interface. The remaining hardware implementations can be found in [8] or [9].

The teleoperation between the master and slave manipulators was engaged by pressing a pushbutton and disengaged by releasing the button. The control parameters for the communication system were chosen as $C = 35.0$, $\Lambda = 1.0$, $A = 64 \times 10^{-6}$, $\kappa_f = 400$ and $\kappa_p = 1.5$, yielding an apparent mass of 1.67 kg and damping of 5.02 Ns/m. Control computations have been run with 500 Hz frequency.

B. Results

In the experiment, the slave manipulator has been driven from free space to contact with the environment along the Cartesian y-axis; see Fig. 5 for the directions of the Cartesian coordinate system. Then, the slave has been instructed to travel a distance of 0.6 m in a constrained motion (contact whilst in motion) along the x-axis. Finally, the slave has been lifted back to free-space motion along the y-axis in flexible environment and back to free space. The environment is flexible in the sense that a set of wooden pallets (see Fig. 5) were placed on rubber mat made of car tires.

Fig. 7 shows the results of the driven experiment. The master manipulator data are shown in blue, and the slave manipulator data in red. *The first column in Fig. 7* shows the *estimated* slave and master forces along the x- and y-axes. In the figure, the master manipulator forces are scaled up by the scaling factor ($\kappa_f = 400$). As the figure shows, accurate force tracking is obtained among the master and slave manipulators, despite the challenges related to the realisation
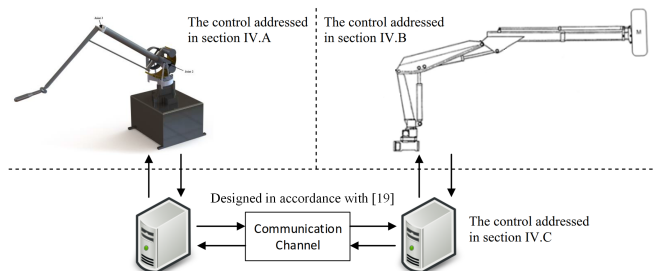
of teleoperation with a hydraulic slave manipulator (see the discussion in Section I). Note that the slave contact forces are estimated from the cylinders' chamber pressures. Thus, some inaccuracies exist in the measured contact forces (see [9] for more details). However, the operator is still able to effectively sense the contact forces between the slave and the environment, and excessive contact forces can be prevented. Furthermore, the force-sensorless approach provides a practical solution for the teleoperation with extremely powerful hydraulic manipulators, as conventional six-DOF force/torque sensors are fragile and prone to overloading.

The second column in Fig. 7 shows the positions of the master and slave manipulators along the Cartesian x- and y-axes. As shown, good position tracking is obtained between the master and the slave. Note that only rather small position scaling was used in the experiment ($\kappa_p = 1.5$), leading to seemingly small motions.

It is valid to mention that this study has demonstrated the preliminary results for the force-reflected bilateral teleoperation with hydraulic manipulators. No major emphasis was given on the tuning of the system parameters and gains. Improvements for tracking results can be expected from a well-tuned system, as demonstrated in our previous research (see [8], [9], [18]). Furthermore, parameter adaptation was used only to adapt the rigid body parameters of the slave manipulator. Extending parameter adaptation to cover more subsystems will overcome remaining parametric uncertainties and further improve the system performance.

VI. CONCLUSIONS

This study has presented a force-reflected bilateral teleoperation between electrical-master and hydraulic slave manipulators. To the authors' best knowledge, this study has presented for the first time a full-dynamics-based teleoperation (i.e., *without any linearisation or order reduction*) with a hydraulic slave. The control design took advantage of the VDC approach, that allowed to design local subsystem-dynamics-based controllers for the master and slave manipulators. Then, the teleoperation system has been completed by designing the communication channel between the master and slave controllers in accordance with [19], which allowed arbitrary motion/force scaling between the manipulators.

Novel features in the paper are the following: 1) realisation of the theory presented in [19] in the full-dynamics-based teleoperation between a table-size electric master manipulator and a heavy-duty hydraulic slave manipulator and 2) a completely force-sensorless teleoperation system (the forces of both manipulators are estimated using dynamical models). The force-sensorless design is a central feature that brings teleoperation closer to heavy-duty hydraulic manipulators as expensive and frail six-DOF force/torque sensors can break easily and, thus are not feasible for heavy-duty operations [8].

The experimental results have demonstrated the advancement of the proposed method and showed excellent motion/force tracking between the manipulators. Similar to our previous studies [8], [9] and [18], tracking performance

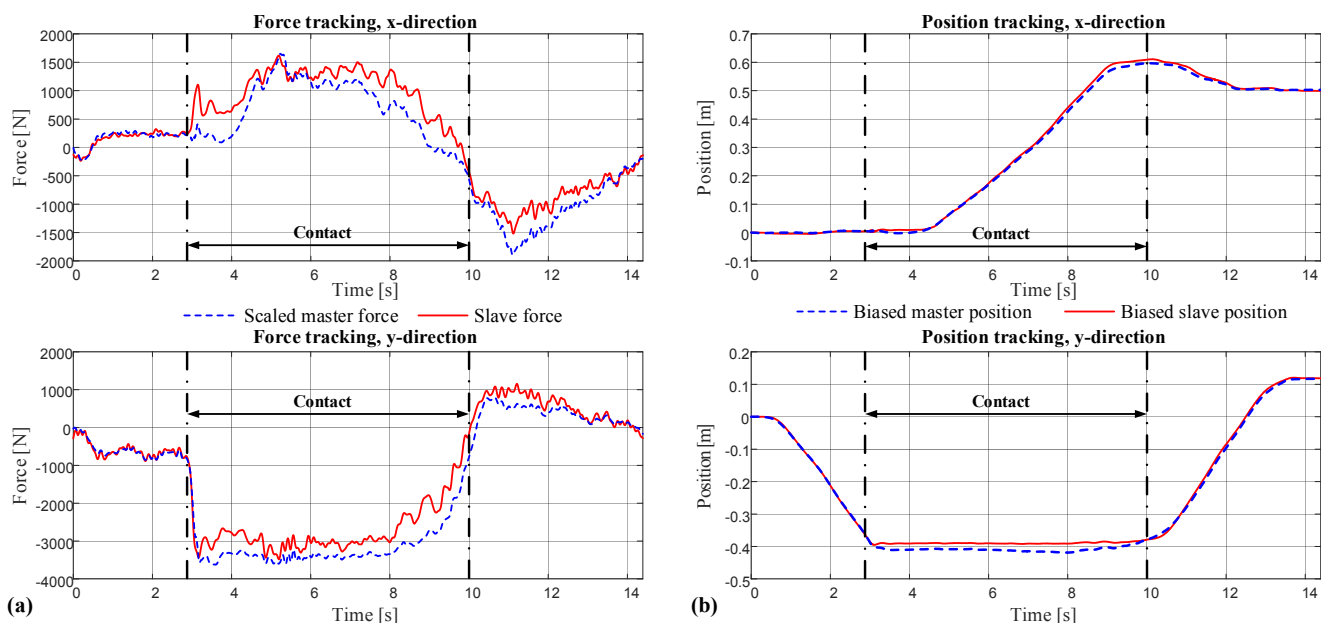Fig. 6.   High-level overview of the experimental implementation.

Fig. 7. Results from experimental implementation with bilateral force-reflected teleoperation. a) Force tracking. b) Position tracking.

improvements can be expected after a rigorous parameter adaptation implementation and throughout tuning of the system parameters.

Our future work consists of further developing the current system by adding parameter adaptation to overcome parametric uncertainties in the dynamics of the master manipulator, the environment and the operator. Furthermore, detailed stability analysis of the system will be shown, and the proposed method will be extended to cover 6-DOF manipulation.

REFERENCES

[1] Eurostat, "Accidents at work statistics." Available at: ec.europa.eu/eurostat/statistics-explained/index.php/Accidents_at_work_statistics (accessed 13.3.2018), 2017.
[2] J. Mattila, J. Koivumäki, D. G. Caldwell, and C. Semini, "A survey on control of hydraulic robotic manipulators with projection to future trends," *IEEE/ASME Transactions on Mechatronics*, vol. 22, pp. 669–680, April 2017.
[3] W.-H. Zhu, *Virtual decomposition control: toward hyper degrees of freedom robots*, vol. 60. Springer Science & Business Media, 2010.
[4] C. H. An and J. M. Hollerbach, "The role of dynamic models in cartesian force control of manipulators," *The International Journal of Robotics Research*, vol. 8, no. 4, pp. 51–72, 1989.
[5] T. Yoshikawa, "Force control of robot manipulators," in *Proc. of IEEE Int. Conf. on Robotics and Automation*, vol. 1, pp. 220–226, 2000.
[6] J.-J. E. Slotine and W. Li, *Applied Nonlinear Control*. Prentice-Hall Englewood Cliffs, NJ, 1991.
[7] M. Krstić, I. Kanellakopoulos, and P. Kokotović, *Nonlinear and Adaptive Control Design*. John Wiley & Sons, Inc., 1995.
[8] J. Koivumäki and J. Mattila, "Stability-guaranteed force-sensorless contact force/motion control of heavy-duty hydraulic manipulators," *IEEE Transactions on Robotics*, vol. 31, pp. 918–935, Aug 2015.
[9] J. Koivumäki and J. Mattila, "Stability-guaranteed impedance control of hydraulic robotic manipulators," *IEEE/ASME Trans. Mechatronics*, vol. 22, no. 2, pp. 601–612, 2017.
[10] P. F. Hokayem and M. W. Spong, "Bilateral teleoperation: An historical survey," *Automatica*, vol. 42, no. 12, pp. 2035 – 2057, 2006.
[11] S. Hirche and M. Buss, "Human-oriented control for haptic teleoperation," *Proceedings of the IEEE*, vol. 100, no. 3, pp. 623–647, 2012.
[12] M. Ostoja-Starzewski and M. Skibniewski, "A master-slave manipulator for excavation and construction tasks," *Robotics and Autonomous Systems*, vol. 4, no. 4, pp. 333 – 337, 1989.

[13] S. Salcudean, K. Hashtrudi-Zaad, S. Tafazoli, S. P. DiMaio, and C. Reboulet, "Bilateral matched-impedance teleoperation with application to excavator control," *IEEE Control Systems*, vol. 19, no. 6, pp. 29–37, 1999.
[14] S. Tafazoli, S. E. Salcudean, K. Hashtrudi-Zaad, and P. D. Lawrence, "Impedance control of a teleoperated excavator," *IEEE Transactions on Control Systems Technology*, vol. 10, pp. 355–367, May 2002.
[15] A. Muhammad *et al.*, "Development of water hydraulic remote handling system for divertor maintenance of ITER," in *IEEE 22nd Symp. on Fusion Engineering*, pp. 1–4, June 2007.
[16] W.-H. Zhu and J. Piedboeuf, "Adaptive output force tracking control of hydraulic cylinders with applications to robot manipulators," *J. Dyn. Syst. Meas. Control*, vol. 127, pp. 206–217, June 2005.
[17] J. Koivumäki and J. Mattila, "High performance non-linear motion/force controller design for redundant hydraulic construction crane automation," *Automation in Construction*, vol. 51, pp. 59–77, 2015.
[18] J. Koivumäki and J. Mattila, "Adaptive and nonlinear control of discharge pressure for variable displacement axial piston pumps," *ASME J. Dyn. Syst., Meas., Control*, vol. 139, no. 10, 2017.
[19] W.-H. Zhu and S. E. Salcudean, "Stability guaranteed teleoperation: an adaptive motion/force control approach," *IEEE Trans. Automatic Control*, vol. 45, pp. 1951–1969, Nov 2000.
[20] W.-H. Zhu, Y.-G. Xi, Z.-J. Zhang, Z. Bien, and J. D. Schutter, "Virtual decomposition based control for generalized high dimensional robotic systems with complicated structure," *IEEE Trans. Robotics and Autom.*, vol. 13, pp. 411–436, Jun 1997.
[21] H. Kazerooni and M.-G. Her, "The dynamics and control of a haptic interface device," *IEEE Trans. Robotics and Autom.*, vol. 10, pp. 453–464, Aug 1994.
[22] J. D. Cooke, "Dependence of human arm movements on limb mechanical properties," *Brain Research*, vol. 165, no. 2, pp. 366–369, 1979.
[23] J. Koivumäki, W.-H. Zhu, and J. Mattila, "Addressing closed-chain dynamics for high-precision control of hydraulic cylinder actuated manipulators." in *Proc. of Bath/ASME Symposium on Fluid Power and Motion Control*, 2018. [Accepted].
[24] P. Malysz and S. Sirouspour, "Nonlinear and filtered force/position mappings in bilateral teleoperation with application to enhanced stiffness discrimination," *IEEE Transactions on Robotics*, vol. 25, pp. 1134–1149, Oct 2009.
[25] P. Malysz and S. Sirouspour, "A kinematic control framework for single-slave asymmetric teleoperation systems," *IEEE Transactions on Robotics*, vol. 27, pp. 901–917, Oct 2011.
[26] D. A. Lawrence, "Stability and transparency in bilateral teleoperation," *IEEE Trans. Robotics and Autom.*, vol. 9, pp. 624–637, Oct 1993.
[27] Y. Yokokohji and T. Yoshikawa, "Bilateral control of master-slave manipulators for ideal kinesthetic coupling-formulation and experiment," *IEEE Trans. Robotics and Autom.*, vol. 10, pp. 605–620, Oct 1994.